Est. 1984

ORIENTAL JOURNAL OF CHEMISTRY
An International Open Access, Peer Reviewed Research Journal

www.orientjchem.org

ISSN: 0970-020 X
CODEN: OJCHEG
2023, Vol. 39, No.(4):
Pg. 933-941

Elevated Polyurethane Coated Polybenzoxaine Intercalated ZrO_2 Nanocomposites: A New Frontier for Protective Coatings in Various Disciplines

VALARMATHI NATARAJ[1], SIVARAJU MANI[2]* and MOHANAMBAL PALANIYAPPAN[3]

[1,3]Department of Chemistry,Vivekanandha college of Arts and Sciences for Women (autonomous) Elayampalayam, Tiruchengode, Namakkal-637205, Tamilnadu, India.
*[2]Department of Chemistry, Thiruvalluvar Govt. Arts college, Rasipuram, Namakkal-637401, Tamilnadu, India.
*Corresponding author E-mail: msivarajuchemistry@gmail.com

http://dx.doi.org/10.13005/ojc/390415

(Received: June 03, 2023; Accepted: July 04, 2023)

ABSTRACT

The suggested polybenzoxine@ZrO_2 nanocomposite surfaces' excellent anticorrosive feature opens in novel avenues for the creation of high action non-corrosive coatings for variety of sectors. The conclusion of mild steel was decreased as a consequence of the accumulation of PBz-wrapped ZrO_2 nanoparticles to the PU coating because they prevented charge transfer at the metal/electrolyte interface. TGA proves that the copolymer matrix's thermodynamic endurance has risen as a result of the ZrO_2 NP addition. EIS findings demonstrated coated PU/PBz@ZrO_2 nanoparticles' exceptional corrosion prevention ability. According to the results of the TEM/EDX analysis, the corrosion products that form at the metal electrolyte interface function as an inactive coating that slows down the breakdown of metals. Because ZrO_2 and PBz work together in harmony, adding polybenzoxazine enhanced ZrO_2 nanoparticles to the polyurethane film strengthens its barrier and mechanical features.

Keywords: ZrO_2 NPs, PU, PBz, Dip Coating, EIS, TEM/EDX, Base pair assessment, Passivation Layer, contact angle, AFM etc.,

INDRODUCTION

Generally materials were used in cars, thermal power stations, railroads and various manufacturing frameworks deteriorate because of deterioration, which causes significant economic loss[1-3]. Many polymeric coverings have been used to extend the life of different metals by preventing them from degrading. Anticorrosive paints and coatings based on synthetic polymer technology are used to protect such devices. In terms of industrial coatings, the polyurethane matrix ranks at the top due to its excellent chemical, physical, thermal, and mechanical characteristics. The polymeric coating has pores that allow corrosive electrons to diffuse through and attack the metal coating, decreasing the coating's ability to withstand erosion. Modern adapted polyurethane films with exceptional

engineering and anticorrosive qualities are the latest innovations that have been created. Due to their affordable price, simple production, electrochemical recurrence and high chemical resistance, Polybenzoxazine polymers have obtained ground-breaking accomplishments in the discipline of protection against corrosion. The capacity of their barrier to form causes cathodic or anodic effects at the metal-coating interaction to change[4,5].

Among the most efficient methods for producing PSC is dip finishing. For effective component emergence, the matrix is submerged in the solution[6]. Following substance deposition, the substrate can be removed by evaporation, creating an independent layer of width[7]. Effort of rigidity, fluid friction, gravitational force, and surface tension are the main forces used in the dip coating procedure[8]. Immersion protecting has the advantages of being inexpensive and having readily adjustable layer thickness. The slow process and potential for blocking the screen are shortcomings of dip covering, which will have a significant effect on the finished product.

When a lack of catalyst is present, phenolic derivatives, which are aldehydes, and basic amines are typically used in the Mannich fusion process to create heterocyclic compounds known as benzoxazine molecules[9]. Since they have exceptional benefits like minimal dielectric properties constants, a high degree of thermal stability, nearly no polymerization shrinking, substantial glass change conditions, minimal exterior liberated energy, a significant carbon remains material, and superhydrophobic exteriors, the associated polybenzoxazines (PBzs) have been a specific kind of thermosetting substances that are often employed in numerous potential applications[10,11].

ZrO_2, TiO_2, SiO_2, Al_2O_3, and other materials have been used in substantial studies to improve the resistivity to corrosion of metallurgical platforms[12,13]. Galvanized steel is protected by a barrier layer made of zirconia, according to Pareja *et al.,*[14]. It efficiently increases the polymer coatings' resistance to the absorption of chlorine ions and noticeably slows the pace of deterioration when used as an additive material. ZrO_2 nanoparticles have exceptional strength in mechanics, thermal insulation, and chemically stable behavior, which makes them very appealing. Very few investigators have studied zirconia nanomaterials' broad variety of spectrum functions, including its use in long-lasting films that are impermeable to erosion. Due to their lack of self-healing powers, coatings made of ZrO_2 nanoparticles do not provide adequate defense in the event that they become damaged[15].

As a consequence, the goal of the present research effort proved to establish extremely durable, affordable, hydrophobic in nature and healing themselves coverings made of polyurethane coating adapted with performing copolymer nanocomposite substances like Polybenzoxazine/ZrO_2 and to examine their electrochemical and anti-corrosive characteristics. We anticipate that the proposed concept will lead towards novel approaches for producing urethane films on conducting polymeric composites for anti-corrosion as well as additional functionalities.

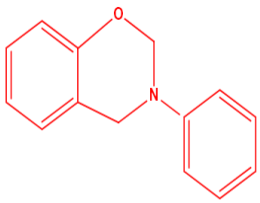

3-methyl-3,4-dihydro-2*H*-benzo[*e*][1,3]oxazine compound with benzene (1:1)

Scheme 1. Structure of Polybenzoxazine

EXPERIMENTAL METHODS

Materials

Before its production, 4-hydroxy -benzaldehyde, Tri-ethoxy silyl propyl amine, Paraformaldehyde 1,4-Dioxane, Ethyl acetate, Sodium hydroxide and Anhydrous sodium sulfate were purchased from Merck Chemicals had been distilled and held at 37°C below the ambient temperature. Polyurethane and ammonium per sulfate were purchased from Merck Chemicals, while extreme quality and scientific level zirconium oxychloride hydrate [$ZrOCl_2.8H_2O$ 99.8%] being purchased through Across Innovations.

A mild steel plate with a width of 1.2mm and the following compositions was utilised as the substrate: S=0.06%, P=0.04%, C=0.18%, Fe= balance and Mn=0.5%. The mild steel specimens' measurements for the dip-coated experiment are 1.2mm x 2mm x 10mm and 1.2mm x 10mm x 10mm, respectively. Following acetone scrubbing

and storage in desiccators, these specimens underwent metallographic refining by being rubbed with emerald sheets of sizes 120, 600, and 800 to achieve a shiny finish.

Synthesis of the ZrO_2 NPs

A zirconia nanoparticles (ZrO_2) was developed from a controlled precipitation procedure[16]. Here the following Precursors were used for synthesis of ZrO_2 nanoparticles such as Zirconium oxychloride hydrate ($ZrOCl_2.8H_2O$) and ammonia solution. At the first step, 0.1 M Zirconium Oxychloride solution 50 mL was prepared using double distilled water and 2.50 M aqueous ammonia solution 50 mL was also prepared in the same water. At the second step, drop wise addition of ammonia solution to $ZrOCl_2.8H_2O$ solution using a vessel and the reaction mixture was stirred rapidly upto the pH was reached to 10 at room temperature. Further, the precipitating agent was added and get a White precipitates of hydroxide form of zirconium. The obtained precipitate of nanoparticles of zirconium(IV) hydroxide was then centrifuged at 3900rpm, washed with water and ethanol. Zirconia powder was obtained from the paste of zirconium(IV) hydroxide was warmed in an autoclave at 100°C for about 12 hours. The formed zirconia powder was calcinated with a muffle furnace at 600°C for about 6 hours. The Obtained nanoparticles are finally confirmed by spectroscopy techniques.

Synthesis of monomer

The 4-hydroxybenzaldehyde, tri-ethoxy silyl propyl amine and paraformaldehyde were dissolved in chloroform were taken in R. B. flask and fixed water condenser in 16 hours. The work completion of the reaction was monitored by thin layer chromatography after finalized it and the reaction mixture was extracted with ethyl acetate washed with 0.1N sodium hydroxide solution, water and brine solution. The organic layer was separated out by separating funnel and dried over anhydrous sodium sulfate solution Finally it was collected as pale yellow oil which was characterized by spectral techniques and called as benzoxazine monomer.

Co-Polymerization process

In situ chemical oxidative polymerization was carried out for the copolymerization with monomer of benzoxazine conducting polymer and absorption of ZrO_2 nanoparticles in copolymer by using oxidant as ammonium persulfate and dopant as Polyurethane. For preparation of polybenzoxazine/ZrO_2 nanocomposite, aqueous mixture of 0.1M benzoxazine monomer, 0.2M Polyurethane and 20 g ZrO_2 nanoparticles was homogeneously mixed using high speed blender at 30-40 min to form an emulsion. By the drop wise addition of aqueous solution of 0.1M ammonium persulfate with continuous stirring for 6-7 h, then obtained copolymerization. Isolation process was used for synthesized copolymer nanocomposite from reaction mixture, cleaning with distilled water to eliminate oligomers and oxidant. The copolymer nanocomposites was formed as paste form which is dried in the vacuum oven at about 60°C[17]

Dip coating process

The derived monomer is solubilized in 1, 4-dioxane and of nano ZrO_2 was incorporated. In that reaction mixture with polyurethane adhesive in toluene has been noted. Polybenzoxazines and polyurethane incorporate with nano ZrO_2) have been organized. The mild steel plate was sanitized utilizing water, hexane, and acetone. The mild steel (ms) was cleaned with emery paper to improve adhesion. Then the MS was dipped in PBz/PU@ Nano ZrO_2 solution for 1 min and systematically removed from the remedy, the cleanup time was around 1 minute. At last, the encased mild steel has been heated and successfully treated at 200°C throughout the furnace for 3 hours. The dipped MS has been further analyzed EIS.

RESULTS AND DISCUSSION

Method of Weight Loss Measurements

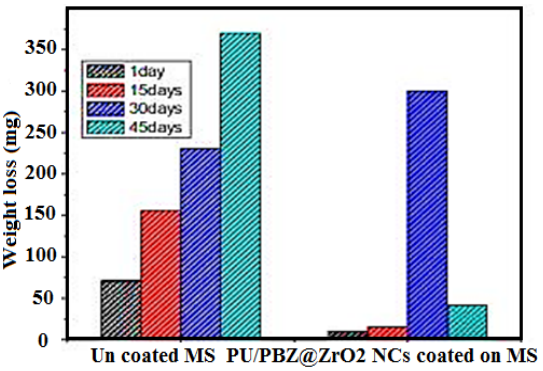

Fig. 1. Corrosion behavior of PU/PBZ@ZrO_2 coated and uncoated MS substrate

Figure 1 gives the cause of time period and corrosion behaviour of PU/PBZ@ZrO_2 coated and uncoated MS substrate. This is very understandable from the outcomes for a given test duration; the weight loss of the PU/PBZ@ZrO_2 coated MS substrate is negligibly lower compared to the uncoated substrate. With increasing test duration, weight loss increases for both PU/PBz@ZrO_2 coated and uncoated MS substrates. However, the weight loss of PU/PBz@ZrO_2 coated MS substrates is very small compared to uncoated substrates at all test durations. The tremendous corrosion resistance of the MS substrate coated with PU/PBz@ZrO_2 is mainly due to the higher corrosion resistance of PU/PBz@ZrO_2. Further, the corrosion rates are also significantly affected by the composite consistency and microstructural changes resulting from the different spray parameters, and it is evident from the microstructure that the developed coatings are free from composite consistency[18].

Crystal phase analysis

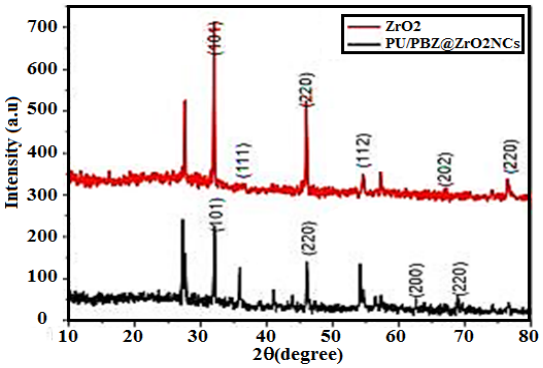

Fig. 2. XRD pattern of ZrO_2 NPs and PU/PBZ@ZrO_2 coated on mild steel in sodium chloride solution

The amorphous nature of copolymer was representing by the weak reflections of Poly (BZ-PU-ZrO_2 NPs) nanocomposites were centered at 2θ values of about 49.1° 56.4°, 65.3° and 78.2° which was viewed in Fig. 2. ZrO_2 NPs has been successfully incorporated in the copolymer matrix from the above mentioned peaks which point out by the observation in Poly (BZ-PU-ZrO_2 NPs) nanocomposites. Fig. 2a shows the XRD pattern of the crystalline zirconia powder. Here four strong diffraction peaks at 2θ=29.88°, 34.43°, 50.01° and 59.67° was observed which is recognized to the formation of the ZrO_2 NPs[40]. Owing to the presence of ZrO_2 NPs, nature of this nanocomposites are crystalline structure from the above mentioned peaks. Fig.2 b also shows the XRD pattern of the crystalline Poly (BZ-PU-ZrO_2NPs). Using Debye Scherrer formula 0.9λ/βcosθ, The average size of the zirconia particles was also determined from the FWHM (full width at half maximum) values of the diffraction peaks. The obtained ZrO_2 nanoparticles approximately crystalline size was expected to be 12nm.

Functional group analysis

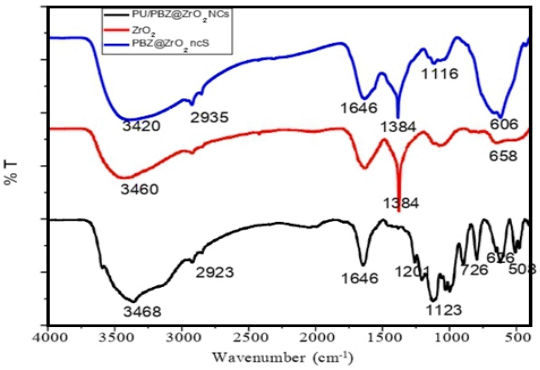

Fig. 3. FTIR pattern of pure ZrO_2 NPs and PU/PBZ@ZrO_2 coated on mild steel in chloride solution

Figure 3 Shows the FTIR spectra of ZrO_2 NPs, PBz@ ZrO_2 NCs and PU/PBz@ ZrO_2 NCs. The characteristic absorption band range was observed at 472 cm^{-1} which was appropriated as a result of Zr-O bond vibrations in ZrO_2[19]. Similarly, these ranges have also been observed in the polymer matrix of the Poly (BZ-PU-ZrO_2 NPs) nanocomposite, indicating that ZrO_2 particles are present within the copolymer matrix. The major individuality of the bands at 1646 and 2923–2935 cm^{-1} are accredited to the stretching modes of C=O and aliphatic C-H vibrations, respectively, while the bands at 1384 cm^{-1} represent the C-N stretching mode of the oxazine ring, which is due to the polymerization of benzoxazine. On because of C-N-C stretching mode which indicates the relations of Polybenzoxazine and benzoxazine portions in the polymer chain, Poly (BZ-ZrO_2 NPs) nanocomposite and Poly (BZ-PU-ZrO_2 NPs) nanocomposite have strong characteristics peaks at 1123 cm^{-1} and 1116 cm^{-1}. A feature broad absorption band at 1646 cm^{-1} is equivalent to vibrations of the absorbed water molecules[20].

Morphological analysis

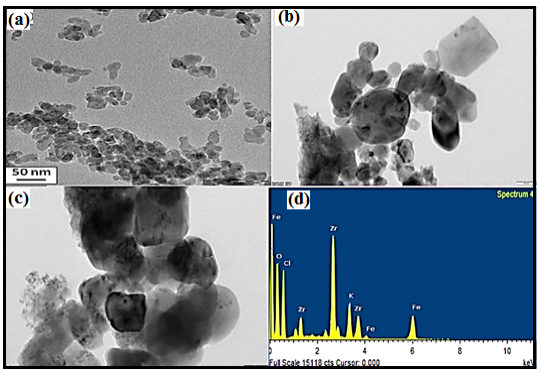

Fig. 4. Shows the TEM micrograph of (a) ZrO_2 NPs, (b) Poly (BZ-ZrO_2 NPs) nanocomposite and Poly(BZ-PU-ZrO_2 NPs) nanocomposite

ZrO_2 particles have a globular shape, as shown by the TEM picture. The Poly(BZ-PU-ZrO_2 NPs) nanocomposite's TEM picture displayed an oval-like shape. According to TEM images, ZrO_2 NPs came across as uniformly discreted throughout the copolymer matrix; this is indicated that they were compatible with the material. The HRTEM Fig. 4 of ZrO_2 NPs revealed that the particles were homogeneous, with a predicted median particle diameter ranging from 10–12nm. These nanoparticles displayed no agglomerated morphology when incorporated into the polymeric matrix, and the estimated diameter of Poly (BZ-PU-ZrO_2 NPs) nanocomposite was approximately 20–24nm.

TGA analysis

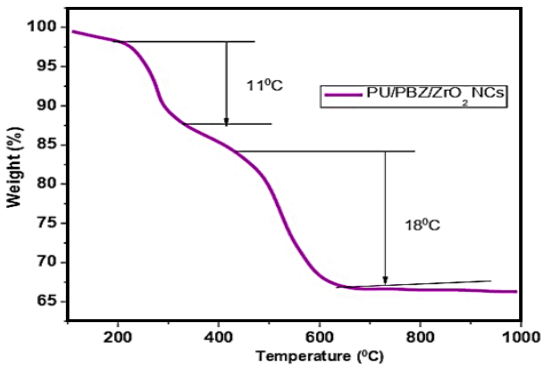

Fig. 5. Shows the TGA curves of Poly(BZ-ZrO_2 NPs) nanocomposite coated on mild steel in chloride medium

The TGA graph of Poly(BZ-PU-ZrO_2 NPs) hybrid shows Fig. 5 that the initially observed loss of weight occurred between 100 and 110°C and was caused by a breakdown in water along with other combustible molecules. The start of the aforementioned chemistry and the aforementioned chemistry is the chemistry. Upon comparing the TGA residues of Poly(BZ-PU-ZrO_2 NPs) nanocomposites, It has been noted that the first stage of weight reduction was the same, while the second phase of losing weight showed some variation. The temperature stability of Poly(BZ-PU-ZrO_2 NPs) nanocomposites was found to be up to 400°C, while that of PBz@ZrO_2 with PU nanocomposites was approximately 600°C. It demonstrates that the addition of ZrO_2 NPs has increased the copolymer matrix's thermodynamic durability.[21,22]

Polarization studies

The anodized and either cathodic graph for a steel substrate covered with MS and PBz@ZrO_2 with PU NCs that was submerged in 3.5% NaCl for after 45 days was shown in Fig. 6. The estimated values for corrosion potential (E_{corr}), corrosion rate (CR), corrosion current density (I_{corr}), and polarisation strength was shown in Table 1.

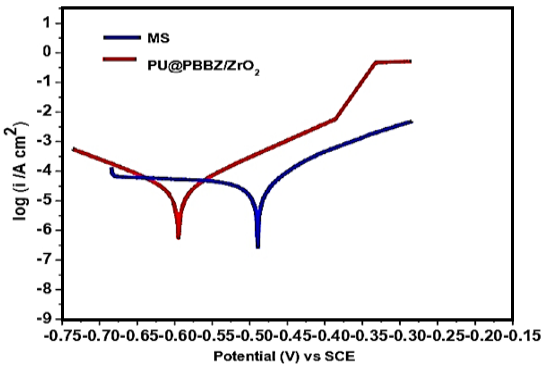

Fig. 6. Shows the polarization studies of poly (BZ-ZrO_2 NPs) nanocomposite coated on MS in base medim

When compared with uncoated mild steel, the rusting potential of the coated specimens was substantially decreased. As the electrical current rate was reduced from 602 to 491mV over the course of after 45 days, the inclusion of PU film improved the polarisation protection of the uncoated mild steel towards rusting compared to 1.831 to 0.257 A/cm^2. After the 45 days immersion, the current density was decreased from 5.95 to 4.85 µA/cm^2. It was observed that the PU–PBz/ZrO_2 nanocomposite added to the PU–PBz/ZrO_2 coating provided a remarkable corrosion resistance with an electron leakage current value of 0.85 A/cm^2 at the time of the coating application. On the other hand, the corrosion current values are slightly increased to 3.20 µA/cm^2 and after 45 days of immersion in base medium, decreases the polarization resistance to 56,432 kΩ cm^2 for mild steel coated with PBz@ZrO_2/PU.

Table 1: Mild steel polarization curves produced by polarization in the presence and absence of various test solutions

Concentration(ppm)	$-E_{corr}$(mV vs SCE)β	βc (mV/dec)β	βa (mV/dec)	$I_{corr}\times10^{-5}$(A/cm^2)	Rp	CR(mmpy)
MS	1060	240.10	655.60	15.75	1455	2.1952
PU/PBZ@ZrO_2 NCs	287	31.59	21.06	03.20	5631	0.0710

Electrochemical impedance spectra

As shown in Fig. 7, uncoated mild steel and coated mild steel with PU/PBz@ZrO_2 in sodium chloride medium are characterized by Nyquist graphs showing the stability and resistance of coatings against corrosive ions on both coated and uncoated nanoparticles of PU/PBz@ZrO_2. These results highlighted to the superior corrosion protection action of coated PU/PBz@ZrO_2 nanoparticles. It is also confirmed from the Table 2 that much impedance is presented for the observation of coatings and it is protectively effect against corrosion. In the presence of coatings, the impedance curves increased with the biggest size viewed in the case of the PU–PBz/ZrO_2 nanocomposite followed by MS. As a consequence, PBz and ZrO_2 have a synergistic effect which enables the PU-PBz/ZrO_2 nanocomposite coating to have superior barrier properties as compared to pure PBz coatings.

Techniques of Atomic Force Microscope (AFM)

The results of the AFM analysis of mild steel coated and uncoated in a 3.5% NaCl solution are shown in Fig. 8a. On the reason of high speed corrosion of MS, uncoated AFM image clearly produce maximum surface roughness at 3.9 µm. As a result of being coated with PU/PBZ@ZrO_2, mild steel morphology differs from mild steel without coatings due to the smoother surface, resulting in maximum surface roughness at 1.9 m for PU/PBZ@ZrO_2 coated mild steel and minimum corrosion is also observed in Fig. 8b. This smoother layer has a noticeably different morphology as a result of the adsorbed coated MS forming a protective layer on top of the layer with a noticeably smoother surface.[23,24]

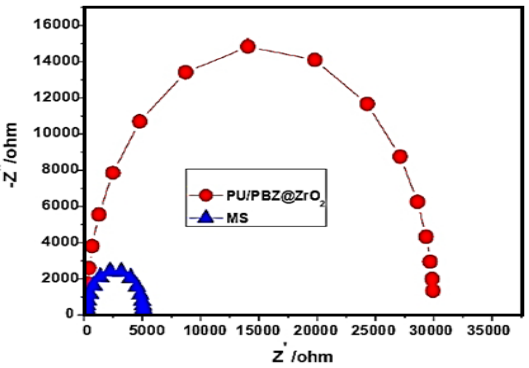

Fig. 7. Nyquist graphs for mild steel dipped in the presence and absence of various test solution produced by AC impedance analysis

Table 2: Based on AC impedance analysis, Nyquist plots for mild steel immersed in various test solutions

Attention/Particulars	R_{ct}(Ω)	Double layer capacitance (C_{dl})	Inhibition efficiency (%)
MS	350.07	2.541	-
PU/PBZ@ZrO_2 NCs	2978.49	0.035	88

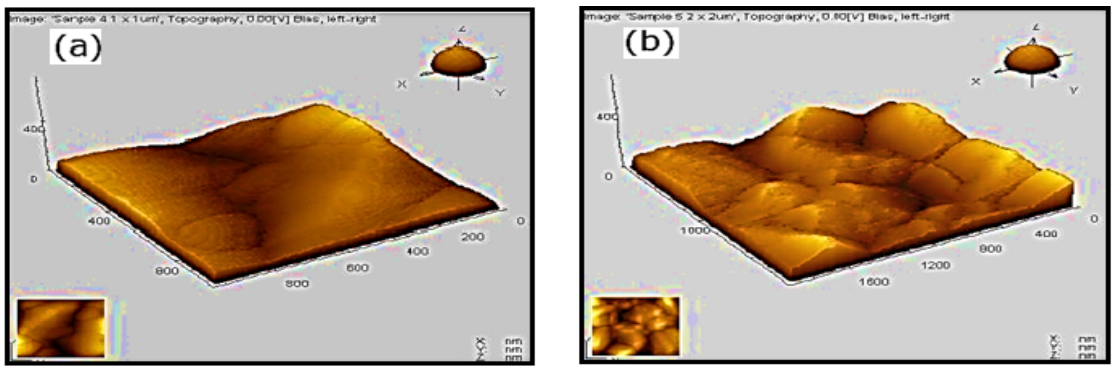

Fig. 8(a). AFM image of mild steel dipped in 3.5% sodium chloride solution & Fig. 8(b). AFM image of MS after coated Dipped in 3.5% sodium chloride solution

Base-pairing assessment

According to the cross cut method, the base-pairing property of the neat PBZ-PU-ZrO_2 NPs and its nanocomposite coatings on MS was evaluated by the crosscut method[25] which was recorded from TEM analysis, and it is shown in Fig. 9. A strong hydrogen bond formed with hydroxyl groups of the mild steel by the connection of the PBZ matrix and the ability of ZrO_2 NPs which is usually, each of the coatings cannot show any peeling after the cross-cutting, representing their strong adhesion to the MS substrate.When compared with the effective PBZ-PU-ZrO_2 NPs and its nanocomposite coating, MNC contents are increasing in their nanocomposites which are successfully enhanced with the smoothness and adhesion of the cutting edge of the coatings.[26]

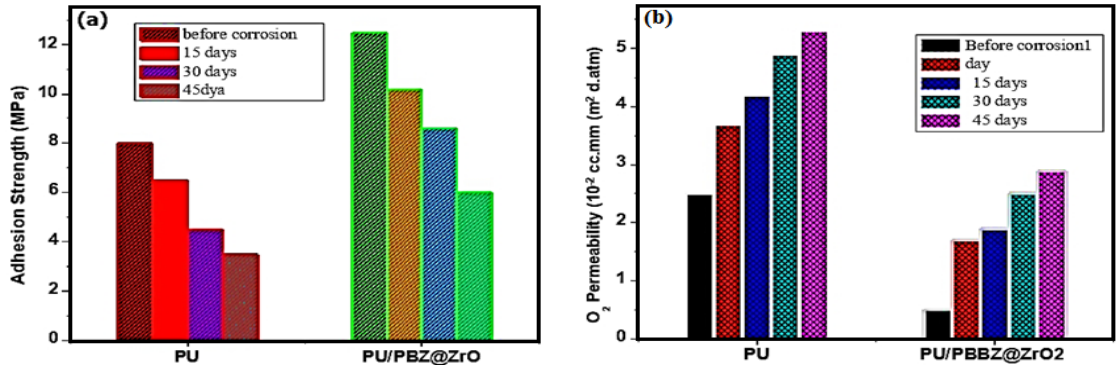

Fig. 9(a). Adhesive strength (b) O2-permeability

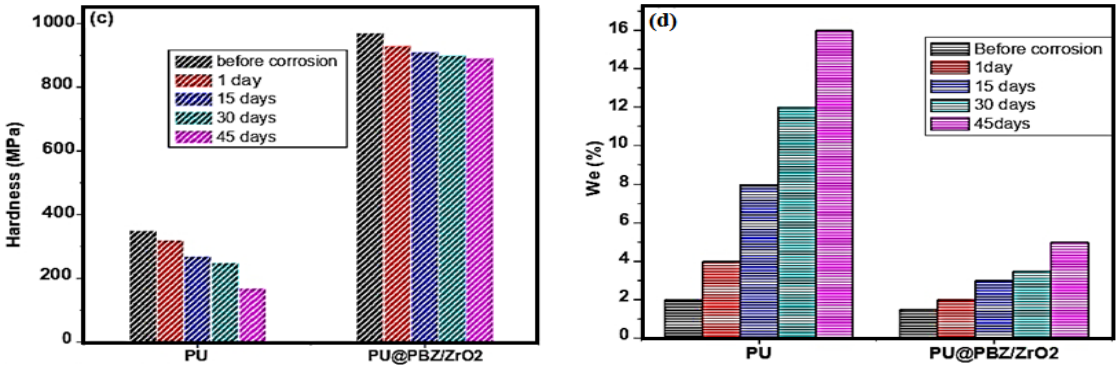

Fig. 9(c). Hardness of steel (d) Water permeability of PU/PBZ@ZrO_2 coated on mild steel in sodium chloride media

Water/oxygen penetration analysis

There is a curve representing the permeability of oxygen in the atmosphere for PU and PU–PBZ/ZrO_2 coated with mild steel dipped in 3.5% sodium chloride is presents in Fig. 10a. A lesser oxygen permeability is achieved in the coatings when PBZ functionalized ZrO_2 nanoparticles are added to PU coatings. As a result of the smaller number of micropores present in the PU@PBZ/ ZrO_2 nanocomposite coating, oxygen is observed to shift less at the metal coating crossing point. Furthermore, the nanocomposite coating also blocks the diffusion of oxygen gas due to the formation of PBZ and ZrO_2 films on the surface of MS.

Contact angle measurement

The graphics obtained for the solitary outdoors falling methodology interactions evaluation of angles are shown in Fig. 10b. This approach can be employed to determine how saturated the coatings on surfaces have grown. a 90-degree angle or smaller for a natural interaction. Hydrophobic, or water-repellent, interfaces are those that have little affinity for flexible, making them less inclined to deteriorate. It has been determined that the exterior interfaces ratios of polymer coatings comprising 4.0 percent by weight of PBz@ZrO_2 with PU hybridized are 102°, implying that the coverings have an impregnable nature. A 78° angle of contact between water molecules and polymers covering was discovered[27,28]. A film composed of PU/PBZ@ ZrO_2's angle of incidence was also measured as an instance of comparison. It was discovered to be

less than 90 degrees which is indicating a greater degree of wetness capability. For the covering will be impenetrable the contact point must be 90 degrees or may be greater. The results thus demonstrate that the hydrophobic characteristics of the outermost coating are increased by the integration of PBZ as a co-monomer in PBZ.

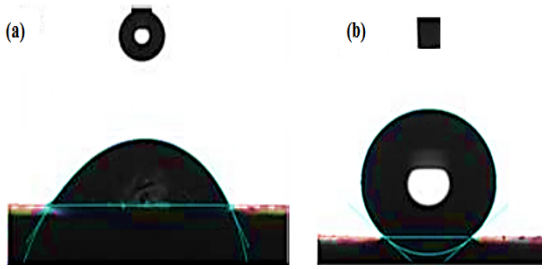

Fig. 10(a). Water oxygen penetration analysis (b) Contact angle of PU/PBZ@ZrO_2 coated on mild steel in sodium chloride media

Barrier from rusting mechanisms

On because of the surface modification of ZrO_2 nanoparticles, the PBZ-PU-ZrO_2 NPs coating is able of shielding the MS from corrosion which is guide with good connecting in the middle of PU and PBZ/ZrO_2. Additionally due to the presence of hydrophobic surface of PBz@ZrO_2 with PU happened by the functionalization of ZrO_2 nanoparticles[29]. So, the PU@PBZ/ZrO_2 nanocomposite coating becomes more difficult than PBZ/ZrO_2 and PU coating across the pierce of corrosive ions via sodium chloride solution which is evidence with the distribution of corrosion ions through the seawater into the coating is inhibited due to the PBz@ZrO_2 with PU coating. This is followed to the improvement in barrier properties of the functionalized with PU-Zirconia nanocomposite coating. The PBz@ZrO_2 with PU coatings observed outstanding barrier properties due to the Polybenzoxazine have lone pair of electrons in the nitrogen and oxygen. When compared the improvement of barrier properties of PBz@ZrO_2 with PU coatings to PU@PBz, PU@ZrO_2, and PU coatings, the lone pair of electron present in the nitrogen and oxygen of PBz was improved. Furthermore, the inclusion of PU-functionalized ZrO_2 nanoparticles with PBz were improved the grip, rigidity, and tensile properties of the nanocomposites as a result of producing a strong chemical bond on the metallic surface[30,31].

CONCLUSION

According to the currently available state of the artistic endeavors, PBz@ZrO_2 with PU nanocomposites that have been effectively deposited on a mild steel exterior, and tests using FTIR, TGA, EDX, and TEM revealed that ZrO_2 nanoparticles were formed and arranged in layers in the polymerization. The coating's consistency in thickness and absence of fissures made it an outstanding corrosion-resistant substance in a saline circumstances, which is how it came to be known. As an outcome, the mild steel that had been covered with PU/PB_Z@ZrO_2 was lesser rusted and had a distinct surface structure with a somewhat rougher interface. According to electrochemical tests, increasing the dimension of the layer that has been absorbed causes an increase in charge transfer resistance (R_t), a drop in the capacitance of the double layer (C_{dl}), and an improvement in corrosive current (I_{corr}) values. According to AC resistance tests, the existence of the PU/PB_Z@ZrO_2 coating material significantly changed the mild steel layer's treatment interaction by forming a protective layer. The ultrahigh hydrophobic characteristics were demonstrated by the examination of fluid interaction distances. For mild steel used in commercial cooling water systems, the PU/PB_Z@ZrO_2 coating technology incorporating PBZ proved more effective at inhibiting rust than ZrO_2. It could provide new opportunities for the use of coastal engineering components that are vulnerable to seawater-induced hastened deterioration.

ACKNOWLEDGEMENT

This research was not received any grant from funding in the public and commercial sectors.

Conflict of Interest

We declare that there is no conflict of interest.

REFERENCES

1. Zhang, S.; Ran, Q.; Fu, Q.; Gu, Y. *Polymer.*, **2019**, *175*, 302–309.
2. Mohamed, M.G.; Hsu, K.C.; Kuo, S.W. *Polym. Chem.*, **2015**, *6*, 2423–2433.
3. Mohamed, M.G.; Kuo, S.W. *Polymers.*, **2016**, *8*, 225.

4. Mohamed, M.G.; Chen, T.C.; Kuo, S.W. *Macromolecules*., **2021**, *54*, 5866–5877 (citation 17 https://pubs. acs.org/doi/abs/10.1021/acs. macromol. 1c00736# cite This)
5. Mohamed, M.G.; Meng, T.S.; Kuo, S.W *Polymer*., **2021**, *226*, 123827 (citation 38).
6. Mohamed, M.G.; Tsai, M.Y.; Wang, C.F.; Huang, C.F; Danko, M.; Dai, L.; Chen, T.; Kuo, S.W. *Polymers.,* **2021**, *13*, 221.
7. Huang, C.F.; Chen, W.H.; Aimi, J.; Huang, Y.S.; Venkatesan, S.; Chiang, Y.W.; Huang, S.H.; Kuo, S.W.; Chen, T. *Polym. Chem*., **2018**, *9*, 5644–5654.
8. Tu, C.W.; Tsai, F.C.; Chang, C.J.; Yang, C.H.; Kuo, S.W.; Zhang, J.; Chen, T.; Huang, C. F. *Polymers*., **2019**, *11*, 631.
9. Mohamed, M.G.; Lin, R.C.; Tu ,J.H.; Lu, F.H.; Hong, J.L.; Jeong, K.U.; Wang, C.F.; Kuo, S.W. *RSC. Adv*., **2015**, *5*, 65635–65645.
10. Ishida, H.; Allen, D. J. *J. Appl. Polym. Sci.,* **2001**, *7*, 406–417.
11. Lin, C.H.; Chang, S.L.; Shen, T.Y.; Shih, Y.S.; Lin, H.T.; Wang ,C.G. *Polym. Chem.,* **2012**, *3*, 935–945.
12. Mohamed, M.G.; Kuo, S.W. *Polymers*., **2019**, *26*, 2019.
13. Qi, H.,Pan, G.; Yin, L.; Zhuang, Y.; Huang, F.; Du, L. *J. Appl. Polym. Sci*., **2009**, *114*, 3026–3033.
14. Lin, R. C.; Mohamed, M. G.; Kuo, S.W. *Macromol. Rapid. Commun.,* **2017**, *38*, 1700251.
15. Mohamed, M.G.; Hsiao, C.H.; Hsu, K.C.; Lu, F.H.; Shih, H.K.; Kuo, S.W. *RSC. Adv*., **2015**, *5*, 12763–12772.
16. Chang, K.C.; Hsu, C.; Lu, H.; Ji ,W.; Chang, C.; Li, W.; Chang, C.H.; Li ,W.Y.; Chuang, T.L.; Yeh, J.M.; Liu, W.R.; Tsai, M.H. *Express. Polym. Lett.,* **2014**, *8*, 243–255.
17. Tripathy, D.K.; Sahoo, B.P. Springer., **2017.**
18. Ruhi, G.; Bhandari, H.; Dhawan, S.K. *Am. J. Polym. Sci*., **2015**, *5*(1A), 18-27.
19. Radhakrishnan, S.; Sonawane, N.; Siju, C.R. Epoxy powder coating containing polyaniline for enhanced corrosion protection. *Prog. Org. Coat*., **2009**, *64*, 383-386.
20. Kumar, A.; Bhandari, H.; Sharma, C.; Khatoon, F.; Dhawan, S.K. *Polym. Int*., **2013**, *62*, 1192-1201.
21. Chang, C.H.; Huang, T.C.; Peng, C.W.; Yeh, T.C.; Lu, H.I.; Hung, W.I.; Weng,C.J.; Yang, T.I.; Yeh, J. M. *Carbon*., **2012**, *50*, 5044-5051.
22. Mahulikar, P.P.; Jadhav, R.S.; Hundiwale, D.G. *Iran. Polym. J*., **2011**, *20*(5), 367-376.
23. Bhandari, H.; Choudhary, V.; Dhawan, S. K. *Synth. Met.,* **2011**, *161*, 753-762.
24. Bhandari, H.; Choudhary, V.; Dhawan, S.K. *Thin Solid Film*., **2010**, *519*(3), 1031-1039.
25. Bagherzadeh, M.R.; Mahdavi, F.M.; Ghasemi, H.S.; Faridi, H.R. *Prog. Org. Coat*., **2010**, *68*, 319-322.
26. Goncalves, G.S.; Baldissera, A.F.; Rodrigues, L.F.; Martini, E.M.A.; Ferreira, C.A. *Synth. Met*., **2011**, *161*, 313-323.
27. Kamaraj, K.; Karpakam, V.; Azim, S.S.; Sathiyanarayanan, S. *Synth. Met*., **2012**, *162*, 536-542.
28. Song, E.; Choi, J.W. *Nanomaterials*., **2013**, *3*, 498-523.
29. Cardoso, M. J. R.; Lima, M. F. S.; Lenz, D. M. *Mat. Res*., **2007**, *10*(4), 425-429.
30. Jadhav, N.; Gelling, V. *J. Coat. Technol. Res*., **2015**, *12*(1), 137-152.
31. Xu, A.; Zhang, F.; Jin, F.; Zhang, R.; Luo, B.; Zhang, T. *Int. J. Electrochem. Sci*., **2014**, *9*, 5116-5125.
32. Jayanthi,K.; Sivaraju,M. *Rasayan. J. Chem*., **2023**, *16*(2), 892-904.